New Journal of Physics
The open access journal for physics

Cascaded second-order surface plasmon solitons due to intrinsic metal nonlinearity

Pavel Ginzburg[1], **Alexey V Krasavin and Anatoly V Zayats**
Department of Physics, King's College London, Strand, London WC2R 2LS, UK
E-mail: pavel.ginzburg@kcl.ac.uk

New Journal of Physics **15** (2013) 013031 (13pp)
Received 12 September 2012
Published 15 January 2013
Online at http://www.njp.org/
doi:10.1088/1367-2630/15/1/013031

Abstract. We theoretically show the existence of cascaded second-order surface plasmon solitons propagating at the interface between a metal and a linear dielectric. Non-local multipole nonlinearities originating from the free conduction electron plasma of the metal lead to strong interaction between co-propagating surface plasmon polariton beams at the fundamental and second-harmonic frequencies. Finite element numerical modelling for an effective two-dimensional medium explicitly demonstrates soliton formation, confirming the theoretical results. The non-diffractive regime of propagation has been demonstrated at a silica/silver interface for 5λ-wide surface plasmon polariton beams with the loss-limited propagation distance of the order of 100 μm for the 750/1550 nm wavelength pair. Plasmon–soliton formation in phase-matched conditions has been shown to be beneficial for non-diffractive surface plasmon polariton propagation.

[1] Author to whom any correspondence should be addressed.

Contents

1. Introduction

One of the most striking phenomena in nonlinear physics is soliton formation. Solitons, wave packets maintaining their shape (spatial or temporal) during propagation, may emerge in various physical systems and were first discovered in narrow water channels [1]. This general nonlinear phenomenon gained considerable attention with the discovery of lasers, which enabled the observation of soliton effects in the optical domain [2, 3]. Solitons can appear in quite a general environment where dispersion is compensated for by nonlinearity, for example, in solids (quantum-mechanical wavepackets) and many-particle biological systems [4]. Temporal solitons in optical fibres have particular applicative implementations as they enable dispersionless propagation of data bit streams over long distances [3]. Spatial solitons may be used for pattern formation in semiconductor lasers and employed for data processing [5]. For further discussion, see the recent comprehensive review on this topic [6]. The second (lowest)-order optical nonlinearity, under certain circumstances, can lead to the formation of temporal and spatial solitons [7].

Nano-optics is a very promising approach for achieving efficient nonlinear interactions, since it enables the manipulation of electromagnetic modes in the near field. Sub-wavelength waveguiding and the field enhancement associated with surface plasmon polariton (SPP) waves supported by materials with negative permittivity can be used for controlling nonlinear interactions [8]. Nonlinear plasmonic phenomena, such as second-harmonic generation, cross- and self-modulation—all enhanced due to the plasmonic field—are sought in active photonic components [9], sensing [10] and signal processing [11]. SPP propagation can be significantly affected by the nonlinearity of the adjacent medium. Nonlinear SPPs at the interface between a metal and a nonlinear Kerr dielectric in the presence of losses have been shown to result in the self-focusing phenomenon with the formation of slowly decaying spatial solitons [12]. When SPPs are guided in a layered metal/nonlinear-dielectric/metal (MIM) structure, hybrid vector spatial plasmon–solitons may emerge. The most striking effect of plasmonics here is when the separation between the two metal claddings of the MIM structure is reduced in order to increase the transverse confinement into the deep sub-wavelength regime, the field envelope in the lateral dimension (bound only by the nonlinearity) is reduced as well [13]. This is the opposite behaviour in comparison with nonlinear all-dielectric waveguides. A partial compensation of the propagation losses of surface plasmon soliton (SPS) in MIM structure was proposed in [14],

where tapering at a properly chosen angle leads to additional field enhancement, thus enabling longer soliton propagation. The combination of gain and loss media, adjusted to metal films, can lead to stable spatial plasmon–solitons formations [15].

While many of the previous studies considered SPP self-focusing phenomena and soliton formation owing to adjacent nonlinear material, metals themselves are very nonlinear. The Kerr-like ponderomotive nonlinearity of noble metals in the infrared spectral range was shown to be comparable with that in highly nonlinear crystals [16]. Parametric optical processes in a metal result from both local interband-based nonlinearity and free-electron plasma-related nonlinearity, and in most cases, from a combination of them. Metal interfaces are also advantageous for the observation of second-order nonlinear processes requiring broken spatial symmetry [8]. The required conditions are simply fulfilled by geometric violation of reflection symmetry at the metal–dielectric interface where SPPs reside. Therefore, there is an opportunity to use the second-order nonlinear effects in metal to control SPP propagation.

Second-order nonlinearity ($\chi^{(2)}$) can lead to spatial solitary wave formation via the effect of second-harmonic generation, as was theoretically predicted [7] and experimentally demonstrated almost two decades ago in potassium titanyl phosphate (KTP) crystals [17] and planar $LiNbO_3$ waveguides [18]. The principle behind such spatial solitons is the collinear propagation of two beams at fundamental and second-harmonic frequencies. These beams exchange their energies via second-order polarizability, which coined the term 'cascaded $\chi^{(2)}$ solitons'. Such an exchange provides the maximum phase delay at the region of high intensity, resulting in self-focusing. This nonlinear phenomenon provides vast opportunities for applications and fundamental studies of soliton effects, as was discussed in a comprehensive review on this topic [19].

In this paper, we demonstrate the concept of cascaded $\chi^{(2)}$ SPSs propagating at the interface between a linear dielectric and a metal with the nonlinearity described by hydrodynamic equations for conduction electron motion, showing that the beam propagation can be described by the effective nonlinear Schrödinger equation. These theoretical predictions are supported by the effective two-dimensional (2D) numerical model, demonstrating soliton formation in an explicit way in the regime of realistic propagation losses with about 100 μm propagation length for the 750/1550 nm wavelength pair. Furthermore, the role of phase matching between the first and the second harmonics on soliton formation has been considered and shown to provide smaller soliton beam widths.

2. Metal nonlinear polarizabilities

Hydrodynamic equations provide a satisfactory description of electrons' dynamics in the conduction band of noble metals such as silver and gold. Traditionally, material susceptibilities, linear as well as nonlinear, are derived with the help of averaged quantities: electron density ($n = n_0 + n_1 e^{-i\omega t} + n_2 e^{-2i\omega t} + \cdots$) and average electron velocity ($v = v_1 e^{-i\omega t} + v_2 e^{-2i\omega t} + \cdots$). The basic result for the linear response is the well-known Drude model, which fits experimental data considerably well away from the plasma frequency and interband transitions. Higher-order corrections and the introduction of additional terms such as quantum pressure and viscosity of electron gas may lead to spatial dispersion contributions and temperature dependence of the appropriate optical constants (see [20] and references therein). Careful inclusion of losses and interband transitions in the framework of the hydrodynamic model provides a more comprehensive but at the same time more complex formulation [21]. Nevertheless, the basic

result of the Sommerfeld free-electron model extension for nonlinear polarization $\vec{P}^{(2)}(\omega, \omega)$ is based on the derivations of Bloembergen *et al* [22], which is in the basis for other advanced models.

Expanding the electromagnetic fields in terms of the fundamental and higher harmonics $\vec{E} = \vec{E}_1 \mathrm{e}^{-\mathrm{i}\omega t} + \vec{E}_2 \mathrm{e}^{-2\mathrm{i}\omega t} + \cdots$, $\vec{H} = \vec{H}_1 \mathrm{e}^{-\mathrm{i}\omega t} + \vec{H}_2 \mathrm{e}^{-2\mathrm{i}\omega t} + \cdots$ and substituting them into hydrodynamic equations, the basic second-harmonic polarization can be derived [22]:

$$\vec{P}^{(2)}_{\mathrm{NL}}(\omega, \omega) = \frac{e\varepsilon_\mathrm{b}\omega_\mathrm{p}^2}{4m\omega^4}(\vec{E}_1 \cdot \vec{\nabla})\vec{E}_1 + \frac{e\varepsilon_\mathrm{b}}{2m\omega^2}(\nabla \cdot \vec{E}_1)\vec{E}_1, \tag{1}$$

where $\omega_\mathrm{p}^2 = n_0 \mathrm{e}^2/m\varepsilon_\mathrm{b}$ is the electron plasma frequency, ω is the field angular frequency, n_0 is the unperturbed electron concentration, m is the electron effective mass and ε_b is the background permittivity. This polarization term describes the frequency doubling. In a similar fashion, the polarization describing the down-conversion process can be derived:

$$\vec{P}^{(2)}_{\mathrm{NL}}(2\omega, -\omega) = -\frac{e\varepsilon_\mathrm{b}}{\omega^2 m}(\nabla \cdot \vec{E}_2)\vec{E}_1^{\,*} + \frac{e\varepsilon_\mathrm{b}}{2\omega^2 m}(\nabla \cdot \vec{E}_1^{\,*})\vec{E}_2. \tag{2}$$

Equations (1) and (2) reveal the possibility of the energy exchange between two co-propagating beams at the frequencies of ω and 2ω through the second-order nonlinearity in metals.

3. Nonlinear equations for general cascaded surface plasmon solitons

The geometrical configuration of co-propagating SPP beams considered in the following is depicted in figures 1(a) and (b). In the linear regime, the SPP modes on the metal–dielectric interface are described by

$$\begin{aligned} &E_i(z,t) = A_i(y,z)\left[\hat{x}e_{ix} + \mathrm{i}\hat{z}e_{iz}\right]\mathrm{e}^{-\mathrm{i}\beta_i z + \mathrm{i}\omega_i t}, \\ &\beta_i = \frac{\omega_i}{c}\sqrt{\frac{\varepsilon_\mathrm{m}(\omega_i)\varepsilon_\mathrm{d}}{\varepsilon_\mathrm{m}(\omega_i)+\varepsilon_\mathrm{d}}}, \\ &k^2_{i\mathrm{d,m}} = \beta_i^2 - \frac{\omega_i^2}{c^2}\varepsilon_{\mathrm{d,m}}, \\ &e_{ix} = \pm\frac{\beta_i}{k_i}\mathrm{e}^{\mp k_i x}, \quad e_{iz} = \mathrm{e}^{\mp k_i x}, \end{aligned} \tag{3}$$

where $i = 1, 2$ corresponds to the waves at the fundamental and second-harmonic frequencies, $A_i(y, z)$ is the spatially-dependent mode amplitude, β_i is the linear propagation constant and $\varepsilon_{\mathrm{d,m}}$ are the linear permittivities of dielectric and metal. Taking into account that the SPP modes are transverse-magnetic (TM)-polarized, the nonlinear wave equation can be decomposed into the x- and z-components, and by subtracting the identities for linear propagation regime, we obtain

$$\begin{aligned} &\partial_{yy}A_i e_{ix}\,\mathrm{e}^{-\mathrm{i}\beta_i z+\mathrm{i}\omega_i t} - \mathrm{i}\,\partial_z A_i \partial_x e_{iz}\,\mathrm{e}^{-\mathrm{i}\beta_i z+\mathrm{i}\omega_i t} - 2\mathrm{i}\,\beta_i \partial_z A_i e_{ix}\,\mathrm{e}^{-\mathrm{i}\beta_i z+\mathrm{i}\omega_i t} - \mu_0 \partial_{tt} P_{\mathrm{NL}\,x} = 0, \\ &\partial_{yy}A_i e_{iz}\,\mathrm{e}^{-\mathrm{i}\beta_i z+\mathrm{i}\omega_i t} + \mathrm{i}\,\partial_z A_i \partial_x e_{ix}\,\mathrm{e}^{-\mathrm{i}\beta_i z+\mathrm{i}\omega_i t} + \mathrm{i}\,\mu_0 \partial_{tt} P_{\mathrm{NL}\,z} = 0, \end{aligned} \tag{4}$$

where ∂_α denotes the derivative with respect to subscript index α and μ_0 is the vacuum permeability (non-magnetic materials were assumed).

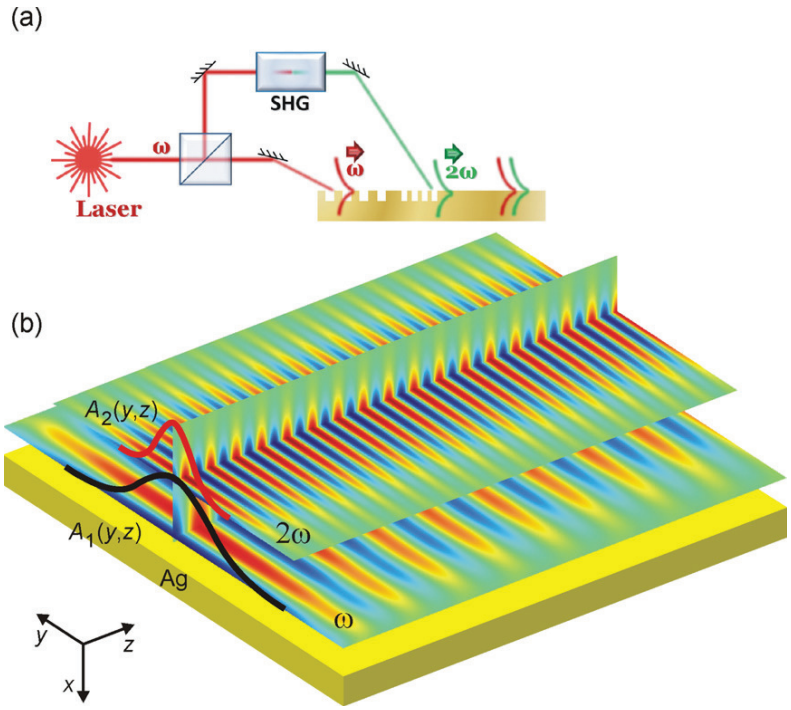

Figure 1. (a) Schematic diagram of a suggested experimental setup: light at the fundamental and second-harmonic frequencies is coupled to the SPPs co-propagating at the interface between a metal and a linear dielectric. (b) Cascaded $\chi^{(2)}$ soliton geometry: co-propagating SPP beams at the fundamental and second-harmonic frequencies can be coupled via the metal nonlinearity. The field distributions of both SPP beams are shown.

Multiplying the set of equations (4) by e_{ix} and e_{iz}, respectively, and summing up the results taking into account the identity for waveguide modes ($e_{ix}\partial_x e_{iz} = e_{iz}\partial_x e_{ix}$), we arrive at

$$\partial_{yy}A_i\,(e_{ix}^2+e_{iz}^2)\,\mathrm{e}^{-\mathrm{i}\beta_i z+\mathrm{i}\omega_i t}-2\mathrm{i}\beta_i\,\partial_z A_i\,e_{ix}^2\,\mathrm{e}^{-\mathrm{i}\beta_i z+\mathrm{i}\omega_i t}-\mu_0\partial_{tt}P_{\mathrm{NL}\,x}e_{ix}+\mathrm{i}\,\mu_0\partial_{tt}P_{\mathrm{NL}\,z}e_{iz}=0. \tag{5}$$

This is a general expression for nonlinear TM modes, similar to the one derived in [12]. Integration over the transverse direction of the waveguide results in

$$\partial_{yy}A_i\left[\int_{-\infty}^{\infty}(e_{ix}^2+e_{iz}^2)\,\mathrm{d}x\right]\mathrm{e}^{-\mathrm{i}\beta_i z+\mathrm{i}\omega_i t}-2\mathrm{i}\beta_i\,\partial_z A_i\left[\int_{-\infty}^{\infty}e_{ix}^2\,\mathrm{d}x\right]\mathrm{e}^{-\mathrm{i}\beta_i z+\mathrm{i}\omega_i t}$$
$$-\mu_0\partial_{tt}\int_{-\infty}^{\infty}(P_{\mathrm{NL}\,x}e_{ix}-\mathrm{i}P_{\mathrm{NL}\,z}e_{iz})\,\mathrm{d}x=0. \tag{6}$$

This set of equations ($i = 1, 2$) describes the self-consistent process of energy exchange between two propagating SPP beams, coupled via any general nonlinear polarizability term.

4. Cascaded surface plasmon solitons originated from hydrodynamic nonlinearity

After derivation of equation (6), the next task is to incorporate the actual nonlinear polarizabilities given by equations (1) and (2). First, we observe that since SPPs are TM modes,

the relation $(\vec{E}\cdot\vec{\nabla})\vec{E} = (\nabla\cdot\vec{E})\vec{E}$ holds simplifying the subsequent derivations. It can be seen that $\nabla\cdot\vec{E}$ is non-vanishing only at the boundary and, in fact, it provides the measure of the polarization charge density at the interface between the metal and dielectric. The integration of equation (6) will eliminate the delta function, corresponding to the surface charge density and will retain the field values in the metal next to the boundary. Typically, far from surface plasmon frequency, the longitudinal (directed along z) component of the SPP field in metal dominates the transverse one by $\sim|\varepsilon_{\mathrm{m}}|$ times (two orders of magnitude in the infrared spectral range) and, hence, may be kept as the source of the leading term in the nonlinear polarization with the other components neglected (they can be taken into account with the mere result of algebraic complications). Defining the nonlinear coefficients $\alpha = (e\varepsilon_{\mathrm{b}}\omega_{\mathrm{p}}^2)/(4m\omega^4) + (e\varepsilon_{\mathrm{b}})/(2m\omega^2)$ and $\beta = (e\varepsilon_{\mathrm{b}})/(2m\omega^2)$, the resulting equations for the fundamental and second-harmonic SPPs can be written as

$$\begin{aligned}
&\partial_{yy}A_1\left[\int_{-\infty}^{\infty}\left(e_{1x}^2+e_{1z}^2\right)\,\mathrm{d}x\right]\mathrm{e}^{-\mathrm{i}\,\beta_1 z+\mathrm{i}\,\omega t} - 2\mathrm{i}\,\beta_1\partial_z A_1\left[\int_{-\infty}^{\infty}e_{1x}^2\,\mathrm{d}x\right]\mathrm{e}^{-\mathrm{i}\,\beta_1 z+\mathrm{i}\,\omega t}\\
&\qquad +\mathrm{i}\,\mu_0\omega^2\beta\left(\frac{\beta_1^*}{k_{1m}^*}-2\frac{\beta_2}{k_{2m}}\right)A_1^*A_2\,\mathrm{e}^{\mathrm{i}(\beta_1-\beta_2)z+\mathrm{i}\,\omega t}=0,\\
&\partial_{yy}A_2\left[\int_{-\infty}^{\infty}\left(e_{2x}^2+e_{2z}^2\right)\,\mathrm{d}x\right]\mathrm{e}^{-\mathrm{i}\,\beta_2 z+\mathrm{i}\,2\omega t} - 2\mathrm{i}\,\beta_2\partial_z A_2\left[\int_{-\infty}^{\infty}e_{2x}^2\,\mathrm{d}x\right]\mathrm{e}^{-\mathrm{i}\,\beta_2 z+\mathrm{i}\,2\omega t}\\
&\qquad +\mathrm{i}\,4\mu_0\omega^2\alpha\frac{\beta_1}{k_{1m}}A_1^2\,\mathrm{e}^{-2\mathrm{i}\,\beta_1 z+\mathrm{i}\,2\omega t}=0.
\end{aligned}\tag{7}$$

Introducing abbreviations $I_i = \int_{-\infty}^{\infty}(e_{ix}^2+e_{iz}^2)\,\mathrm{d}x$, $I_{Xi} = \int_{-\infty}^{\infty}e_{ix}^2\,\mathrm{d}x$, $N_1 = \mathrm{i}\,\mu_0\omega^2\times\beta\left(\frac{\beta_1^*}{k_{1m}^*}-2\frac{\beta_2}{k_{2m}}\right)$, $N_2 = \mathrm{i}\,4\mu_0\omega^2\alpha\frac{\beta_1}{k_{1m}}$ and $\Delta = 2\beta_1-\beta_2$, we rearrange the set of equations (7) as

$$\begin{aligned}
&\partial_{yy}A_1I_1 - 2\mathrm{i}\,\beta_1\partial_z A_1 I_{X1} + N_1A_1^*A_2\mathrm{e}^{\mathrm{i}\,\Delta z}=0,\\
&\partial_{yy}A_2I_2 - 2\mathrm{i}\,\beta_2\partial_z A_2 I_{X2} + N_2A_1^2\mathrm{e}^{\mathrm{i}\,\Delta z}=0.
\end{aligned}\tag{8}$$

Assuming also a large momentum mismatch between the fundamental and second-harmonic SPPs (approximation of [23]) which may usually be justified due to the SPP dispersion, we can show that the second equation of the set of equations (8) will result in

$$A_2 = \frac{N_2\,\mathrm{e}^{-\mathrm{i}\Delta z}}{2\beta_2\Delta I_{X2}}A_1^2.\tag{9}$$

Substituting this amplitude back into the first equation in the set of equations (8), we obtain

$$\frac{I_1}{2\beta_1 I_{X1}}\partial_{yy}A_1 - \mathrm{i}\,\partial_z A_1 + \frac{N_2N_1}{4\beta_2\beta_1\Delta I_{X1}I_{X2}}|A_1|^2A_1=0,\tag{10}$$

which is the final result of our derivations. Equation (10) is the nonlinear Schrödinger equation (NLSE) describing the nonlinear propagation of the first-harmonic (fundamental) SPP mode on the surface of the metal exhibiting second-order nonlinearity, with a possible solution corresponding to a solitary wave. It is the most general tool for soliton description, and its

coefficients indicate whether solitons can emerge. Even though the derivations rely on the large momentum mismatch, the final result for the effective nonlinear coefficient in equation (10) singularly grows close to the phase-matching condition, indicating its possible advantage.

5. Numerical simulations

To further investigate the nonlinear interaction between the SPP signals, finite-element numerical simulations were employed. SPP modes are strongly confined to the metal–dielectric interface where the nonlinear interactions take place. For the sake of numerical simplicity, we have studied a general 2D model of cascaded $\chi^{(2)}$ solitons for which the signal dependence on the x-coordinate was omitted, qualitatively not affecting the results, since x is a dummy variable in equation (10). At the same time, the mismatch between the effective refractive indices for the fundamental and the double-frequency beams, reflecting the dispersion of the SPP waves and determining the essential phase relations between the waves, was taken into account. The finite propagation distance of SPPs, which is determined by Ohmic losses in the metal, was also taken into account.

Initially, we studied the linear regime of SPP propagation at the silica/silver interface with $\varepsilon_1^{\mathrm{Ag}} = -120 + 3\mathrm{i}$, $\varepsilon_2^{\mathrm{Ag}} = -27 + 0.32\mathrm{i}$ at $\lambda_1 = 1500\,\mathrm{nm}$ and $\lambda_2 = 750\,\mathrm{nm}$, respectively [24]. In this case, the SPP refraction indices for the simulated effective medium for the first and second harmonics are $n_1^{\mathrm{eff}} = 1.457 + 3.25 \times 10^{-4}\mathrm{i}$ and $n_2^{\mathrm{eff}} = 1.514 + 7.5 \times 10^{-4}\,\mathrm{i}$, corresponding to the mismatch between the wavevectors of approximately 3.8% and the SPP propagation lengths of 370 and 80 μm, respectively. At the excitation boundary ($z = 0$), the SPP beams at the fundamental and second-harmonic frequencies were set to propagate collinearly along the z-axis with the transverse profile described by the Gaussian distributions $E_{1,2}(y, 0) \sim A_{1,2}(y, 0) \sim \exp(-y^2/w_{1,2}^2)$ with half-widths of $w_{1,2} = 2.5\lambda_{1,2}$. Their spatial evolution was then studied. The intensity distributions $|E_{1,2x}|^2$ obtained in the linear (uncoupled) regime show typical diffraction-governed propagation for both fundamental and second-harmonic SPP beams (figures 2(a) and (e)).

To prove the soliton formation resulting from the derived hydrodynamic model in a more general case of arbitrary modal dispersion (equation (10) is a particular case when $\Delta \gg 0$), we have introduced into the material polarization the corresponding nonlinear terms $P_{1,\mathrm{NL}} = \chi^{(2)}(E_1)^* E_2$ and $P_{2,\mathrm{NL}} = 1/2 \cdot \chi^{(2)}(E_1)^2$ assuming the excitation field amplitudes for both harmonics to be the same $E_1 = E_2$. It should be noted that the amplitudes of the fundamental and the second-harmonic SPP waves are connected in the solitonic regime via equation (9), and the choice of the relative amplitudes of the two waves is not important as they adjust themselves to reach the required ratio. The nonlinear interaction was gradually increased to $\chi^{(2)} E_1 = 0.02$, resulting in the intensity distributions shown in figures 2(b) and (f) where deviations from the linear propagation regime are observed. Further increase of the field to $\chi^{(2)} E_1 = 0.05$ leads to even more pronounced deviations from the diffractive propagation regime (figures 2(c) and (g)). The observed intensity fringes are defined by the mismatch between the SPP effective refraction indices at the two frequencies. At the same time, the energy exchange between the beams can be seen: the maximum intensity of one beam corresponds to the minimum intensity of the other (cf cross sections B and C in (c) and (g)). The same effect can be seen in the actual intensity plots along these cross sections (graphs (d) and (h)). Furthermore, the effect of narrowing of the SPP beams, driven by the nonlinearity, can be seen in the decrease in the average beam width $\frac{1}{2}(w_{1,B} + w_{1,C})/w_{1,A} = 0.94$ for the fundamental frequency and $\frac{1}{2}(w_{2,B} + w_{2,C})/w_{2,A} = 0.8$ for

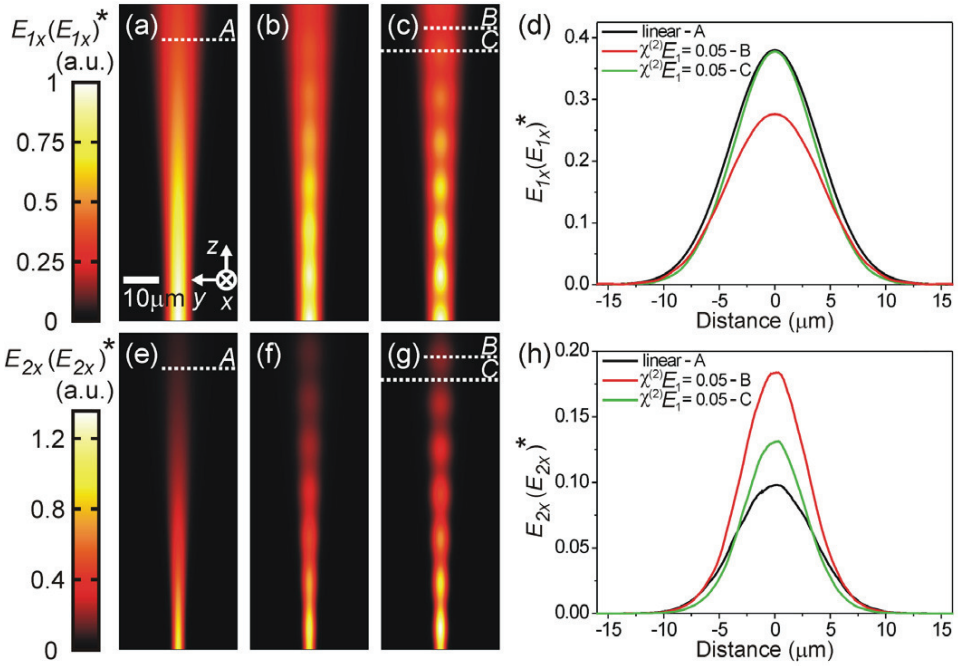

Figure 2. Linear propagation of (a) the fundamental and (e) the second-harmonic SPP beams in effective 2D medium (Au/silica interface) with the effective indices $n_1^{\text{eff}} = 1.457 + 3.25 \times 10^{-4}\,\text{i}$ and $n_2^{\text{eff}} = 1.514 + 7.5 \times 10^{-4}\,\text{i}$ at 1500 and 750 nm wavelengths, respectively. Nonlinear propagation and self-focusing of (b, c) the fundamental and (f, g) the second-harmonic SPP beams for different light intensities corresponding to (b, f) $\chi^{(2)}E_1 = 0.02$ and (c, g) $\chi^{(2)}E_1 = 0.05$ nonlinearities. The initial amplitudes of both beams are equal ($E_1 = E_2$) and the beam half-widths are $w_{1,2} = 2.5\lambda_{1,2}$. The graphs (d) and (g) show the intensity plots along cross sections indicated in (a, c) and (e, g), respectively.

the double frequency, where w_B and w_C are the interchanging maximum/minimum of SPP beam widths in the solitonic regime, and w_A is the beam width in the linear (non-interacting) propagation regime at the same average distance. It should be noted that the largest modulation of the intensity profiles is in the centres of the beams, where intensities are highest and nonlinear coupling is strongest.

One of the assumptions made prior to derivation of equation (9) is the large wavevector mismatch between the fundamental and second-harmonic SPPs. At the same time, the nonlinear coefficient $(N_2N_1)/(4\beta_2\beta_1\Delta I_{X1}I_{X2})$ in this equation has the mismatch term Δ in the denominator and, hence, is larger for smaller mismatches. In these circumstances, the numerical simulations provide a vital opportunity to extend the analytical theory and to address the particularly interesting scenario when the mismatch is zero so that the phase-matching conditions are realized.

Phase matching between the fundamental and second-harmonic SPPs can be obtained by introducing at the SPP-supporting interface dielectric having anomalous dispersion [25] to compensate for the SPP dispersion. Adjusting the glass composition to $5\,TiO_2$–$55\,SiO_2$–$40\,Na_2O$, it is possible to achieve a match between the real parts of the effective refractive indices

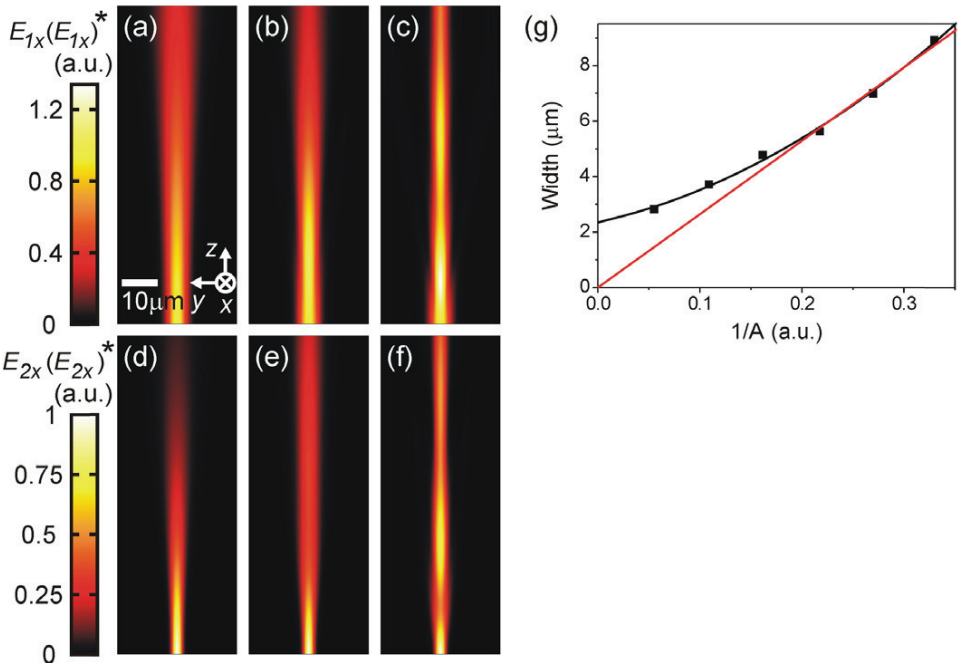

Figure 3. Linear propagation of (a) the fundamental and (d) the second-harmonic SPP beams at Au/dielectric interface with equal parts of the effective indices $n_1^{\text{eff}} = 1.583 - 4.16 \times 10^{-4}\text{i}$, $n_2^{\text{eff}} = 1.583 - 8.6 \times 10^{-4}\text{i}$. Nonlinear propagation and self-focusing of (b, c) the fundamental and (e, f) the second-harmonics SPP beams for different light intensities corresponding to (b, e) $\chi^{(2)}E_1 = 0.02$ and (c, f) $\chi^{(2)}E_1 = 0.05$. The amplitudes of both beams are equal ($E_1 = E_2$) and the beam half-widths are $w_{1,2} = 2.5\lambda_{1,2}$. (g) The dependence of the soliton width on its inverse amplitude at constant nonlinearity: the symbols present numerical data, the black line is a guide to the eye and the red line is the theoretical fit using equation (10).

$\text{Re}(n_1^{\text{eff}}) = \text{Re}(n_2^{\text{eff}}) = 1.583$. The evolution of the SPP beams for the linear and nonlinear cases at this interface was then studied. The resulting intensity maps are presented in figure 3. One can clearly see the evident transformation of the SPP modes into highly localized non-diffracting solitons. Moreover, in this case, the nonlinearity allows us to achieve SPP beams with a narrow spatial profile; the self-focusing effect occurring near the excitation boundary can also be seen (figures 3(c) and (f)).

6. Discussion

The general solution of the NLSE predicts certain relations between soliton amplitude (A), width (w) and effective cubic nonlinearity of the medium. Applying this property to the cascaded soliton described by equation (10), the following relation should hold: $Aw\tilde{\chi}^{(2)} = \text{const}$, where $\tilde{\chi}^{(2)} \sim \sqrt{\alpha\beta}$ is the geometrical average of the second-harmonic and down-conversion susceptibilities. In order to check the validity of this relation, we have

performed numerical studies, observing the relation between A and w while keeping the nonlinearity constant. Figure 3(g) shows the resulting dependence of the soliton width on its inverted amplitude. The numerical data follow the analytical predictions when the soliton width is larger than the classical diffraction limit. However, for the transversal beam dimensions of the order of the wavelength, significant deviations from linear dependence have been observed.

Addressing the possibility for experimental demonstration of the proposed phenomenon and taking into account the measured values of metal nonlinearities, we have estimated the required optical intensities and compared them with damage thresholds. The laser-induced damage thresholds of thin metal films are strongly dependent on the quality of the surface. The damage fluence for high-quality silver mirrors is of the order of $0.3\,\mathrm{J\,cm^{-2}}$ for 50 fs pulses at 800 nm wavelength. The reported surface nonlinearity of the metal is of the order of $30 \times 10^{-14}\,\mathrm{cm^2}$ per statvolt [26], and the field amplitudes needed for soliton generation are less than $1\,\mathrm{GV\,m^{-1}}$, which is still significantly less than the damage threshold. The increase of transversal dimensions of the soliton will reduce its amplitude (figure 3(g)), pushing the required intensity even further away from the damage threshold. Moreover, surface patterning may effectively increase overall nonlinearity by employing structures with on-demand optical response [27], which could provide resonances at both fundamental and second-harmonic frequencies, thus maximizing the efficiency of the nonlinear interactions [28]. Various types of plasmonic waveguides, e.g. metal–insulator–metal structures [29], may be considered and could further reduce the required intensities for cascaded plasmon–soliton formation.

The soliton generation proposed and described above occurs at continuous (unstructured) metal surfaces. However, a very remarkable and application-promising phenomenon of diffraction compensation could emerge in discrete systems that can be realized, e.g., in an array of coupled waveguides. In the linear propagation regime, the optical energy will spread away from the waveguide where it was initially launched due to electromagnetic coupling to the neighbouring waveguides. However, in the presence of nonlinearity in the coupled waveguide system, the energy spreading can be compensated for and discrete solitons could emerge [30]. Various photonic realizations of this phenomenon [31] and remarkable optical analogues of quantum effects [32] have been demonstrated. Plasmonic counterparts of the discrete soliton phenomenon have also been studied in arrays of planar [33], wire [34] waveguides and square lattice of nanowires supporting vortical plasmonic lattice solitons [35].

Besides the nonlinear approach for diffractionless propagation of waves, it is worthwhile to mention linear methods to obtain similar behaviour. The most widely known examples here are Bessel [36] and Airy [37] beams, which maintain their profiles along the propagation direction, but relying on an infinite number of side lobes. However, even with a limited transverse size, diffractionless propagation may be obtained with a good approximation. Theoretical predictions were supported by many optical experiments, among them free-space Airy beams [38], their SPP counterpart [39] and SPP beams with controllable trajectories [40]. Other interesting difractionless surface waves, such as cosine-Gauss type [41] and spatially accelerating waves [42], were experimentally demonstrated, as well as bulk non-paraxial realizations [43, 44]. While these linear approaches do not require high powers, they need a specific complex sub-wavelength structuring of the surface (or spatial amplitude modulation) in contrast with nonlinear diffractionless solitons, which can be achieved on unstructured metal interfaces.

7. Summary

We have derived the NLSE describing the SPP soliton formation in the cascaded second-order nonlinearity regime. The nonlinearity originates from the presence of the metal interface and is derived using the hydrodynamic description of free-electron plasma. Finite-element simulations performed with rigorously introduced second-order coupling between the fundamental and the second-harmonic beams confirm the formation of cascaded plasmon solitons, underlining the benefits of phase matching for non-diffractive SPP propagation over distances of hundreds of microns.

Acknowledgments

This work was partially supported by the EPSRC (UK). PG acknowledges the Royal Society for a Newton International Fellowship. The authors thank Professor Dmitry Skryabin for discussions.

References

[1] Russell J S 1844 Report on waves *Fourteenth Meeting of the British Association for the Advancement of Science*
[2] Bjorkholm J E and Ashkin A 1974 CW self-focusing and self-trapping of light in sodium vapor *Phys. Rev. Lett.* **32** 129–32
[3] Kivshar Y S and Agrawal G 2003 *Optical Solitons: From Fibers to Photonic Crystals* (New York: Academic)
[4] Akhmediev N and Ankiewicz A 2008 *Dissipative Solitons: From Optics to Biology and Medicine* (Berlin: Springer)
[5] Ackemann T, Firth W J and Oppo G L 2009 Fundamentals and applications of spatial dissipative solitons in photonic devices *Advances in Atomic Molecular and Optical Physics* vol 57, ed P R B E Arimondo and C C Lin (New York: Academic) chapter 6, pp 323–421
[6] Chen Z, Segev M and Christodoulides D N 2012 Optical spatial solitons: historical overview and recent advances *Rep. Prog. Phys.* **75** 086401
[7] Karamzin Yu N and Sukhorukov A P 1976 Mutual focusing of high-power light beams in media with quadratic nonlinearity *Sov. Phys.—JETP* **41** 414–20
[8] Kauranen M and Zayats A V 2012 Nonlinear plasmonics *Nature Photon.* **6** 737–48
[9] Krasavin A V, Vo T P, Dickson W, Bolger P M and Zayats A V 2011 All-plasmonic modulation via stimulated emission of copropagating surface plasmon polaritons on a substrate with gain *Nano Lett.* **11** 2231–5
[10] Anker J N, Hall W P, Lyandres O, Shah N C, Zhao J and Duyne R P V 2008 Biosensing with plasmonic nanosensors *Nature Mater.* **7** 442–53
[11] MacDonald K F, Sámson Z L, Stockman M I and Zheludev N I 2009 Ultrafast active plasmonics *Nature Photon.* **3** 55–8
[12] Davoyan A R, Shadrivov I V and Kivshar Y S 2009 Self-focusing and spatial plasmon-polariton solitons *Opt. Express* **17** 21732–7
[13] Feigenbaum E and Orenstein M 2007 Plasmon soliton *Opt. Lett.* **32** 674–6
[14] Davoyan A R, Shadrivov I V, Zharov A A, Gramotnev D K and Kivshar Y S 2010 Nonlinear nanofocusing in tapered plasmonic waveguides *Phys. Rev. Lett.* **105** 116804
[15] Marini A, Skryabin D V and Malomed B 2011 Stable spatial plasmon solitons in a dielectric–metal–dielectric geometry with gain and loss *Opt. Express* **19** 6616–22

[16] Ginzburg P, Hayat A, Berkovitch N and Orenstein M 2010 Nonlocal ponderomotive nonlinearity in plasmonics *Opt. Lett.* **35** 1551–3
[17] Torruellas W E, Wang Z, Hagan D J, VanStryland E W, Stegeman G I, Torner L and Menyuk C R 1995 Observation of two-dimensional spatial solitary waves in a quadratic medium *Phys. Rev. Lett.* **74** 5036–9
[18] Schiek R, Baek Y and Stegeman G I 1996 One-dimensional spatial solitary waves due to cascaded second-order nonlinearities in planar waveguides *Phys. Rev.* E **53** 1138–41
[19] Torner L and Barthelemy A 2003 Quadratic solitons: recent developments *IEEE J. Quantum Electron.* **39** 22–30
[20] Sipe J E, So V C Y, Fukui M and Stegeman G I 1980 Analysis of second-harmonic generation at metal surfaces *Phys. Rev.* B **21** 4389–402
[21] Scalora M, Vincenti M A, de Ceglia D, Roppo V, Centini M, Akozbek N and Bloemer M J 2010 Second- and third-harmonic generation in metal-based structures *Phys. Rev.* A **82** 043828
[22] Bloembergen N, Chang R K, Jha S S and Lee C H 1968 Optical second-harmonic generation in reflection from media with inversion symmetry *Phys. Rev.* **174** 813–22
[23] Menyuk C R, Schiek R and Torner L 1994 Solitary waves due to $\chi^{(2)}$: $\chi^{(2)}$ cascading *J. Opt. Soc. Am.* B **11** 2434–43
[24] Johnson P B and Christy R W 1972 Optical constants of the noble metals *Phys. Rev.* B **6** 4370–9
[25] Abdel-Baki M, Abdel Wahab F A and El-Diasty F 2006 Optical characterization of $x\mathrm{TiO_2}$–$(60-x)\mathrm{SiO_2}$–$40\,\mathrm{Na_2O}$ glasses: I. Linear and nonlinear dispersion properties *Mater. Chem. Phys.* **96** 201–10
[26] Wang F X, Rodríguez F J, Albers W M, Ahorinta R, Sipe J E and Kauranen M 2009 Surface and bulk contributions to the second-order nonlinear optical response of a gold film *Phys. Rev.* B **80** 233402
[27] Ginzburg P, Berkovitch N, Nevet A, Shor I and Orenstein M 2011 Resonances on-demand for plasmonic nano-particles *Nano Lett.* **11** 2329–33
[28] Ginzburg P, Krasavin A, Sonnefraud S, Murphy A, Pollard R J, Maier S A and Zayats A V 2012 Nonlinearly coupled localized plasmon resonances: resonant second-harmonic generation *Phys. Rev.* B **86** 085422
[29] Ginzburg P, Arbel D and Orenstein M 2006 Gap plasmon polariton structure for very efficient microscale to nanoscale interfacing *Opt. Lett.* **31** 3288–90
[30] Christodoulides D N, Lederer F and Silberberg Y 2003 Discretizing light behaviour in linear and nonlinear waveguide lattices *Nature* **424** 817–23
[31] Fleischer J W, Segev M, Efremidis N K and Christodoulides D N 2003 Observation of two-dimensional discrete solitons in optically induced nonlinear photonic lattices *Nature* **422** 147–50
[32] Morandotti R, Peschel U, Aitchison J S, Eisenberg H S and Silberberg Y 1999 Experimental observation of linear and nonlinear optical bloch oscillations *Phys. Rev. Lett.* **83** 4756–9
[33] Liu Y, Bartal G, Genov D A and Zhang X 2007 Subwavelength discrete solitons in nonlinear metamaterials *Phys. Rev. Lett.* **99** 153901
[34] Ye F, Mihalache D, Hu B and Panoiu N C 2010 Subwavelength plasmonic lattice solitons in arrays of metallic nanowires *Phys. Rev. Lett.* **104** 106802
[35] Ye F, Mihalache D, Hu B and Panoiu N C 2011 Subwavelength vortical plasmonic lattice solitons *Opt. Lett.* **36** 1179–81
[36] Durnin J, Miceli J J and Eberly J H 1987 Diffraction-free beams *Phys. Rev. Lett.* **58** 1499–501
[37] Berry M V and Balazs N L 1979 Nonspreading wave packets *Am. J. Phys.* **47** 264–7
[38] Siviloglou G A, Broky J, Dogariu A and Christodoulides D N 2007 Observation of accelerating Airy beams *Phys. Rev. Lett.* **99** 213901
[39] Li L, Li T, Wang S M, Zhang C and Zhu S N 2011 Plasmonic Airy beam generated by in-plane diffraction *Phys. Rev. Lett.* **107** 126804
[40] Zhang P, Wang S, Liu Y, Yin X, Lu C, Chen Z and Zhang X 2011 Plasmonic Airy beams with dynamically controlled trajectories *Opt. Lett.* **36** 3191–3

[41] Lin J, Dellinger J, Genevet P, Cluzel B, de Fornel F and Capasso F 2012 Cosine-Gauss plasmon beam: a localized long-range nondiffracting surface wave *Phys. Rev. Lett.* **109** 093904

[42] Kaminer I, Bekenstein R, Nemirovsky J and Segev M 2012 Nondiffracting accelerating wave packets of Maxwell's equations *Phys. Rev. Lett.* **108** 163901

[43] Zhang P, Hu Y, Li T, Cannan D, Yin X, Morandotti R, Chen Z and Zhang X 2012 Nonparaxial Mathieu and Weber accelerating beams *Phys. Rev. Lett.* **109** 193901

[44] Zhang P, Hu Y, Cannan D, Salandrino A, Li T, Morandotti R, Zhang X and Chen Z 2012 Generation of linear and nonlinear nonparaxial accelerating beams *Opt. Lett.* **15** 2820–2